Journal of Zhejiang University SCIENCE A
ISSN 1009-3095 (Print); ISSN 1862-1775 (Online)
www.zju.edu.cn/jzus; www.springerlink.com
E-mail: jzus@zju.edu.cn

Numerical prediction of vortex flow and thermal separation in a subsonic vortex tube

SMITH Eiamsa-ard[1], PONGJET Promvonge[‡2]

([1]*Department of Mechanical Engineering, Faculty of Engineering, Mahanakorn University of Technology, Bangkok 10530, Thailand*)

([2]*Department of Mechanical Engineering, Faculty of Engineering, King Mongkut's Institute of Technology Ladkrabang, Bangkok 10520, Thailand*)

E-mail: smith@mut.ac.th; kppongje@kmitl.ac.th

Received Dec. 5, 2005; revision accepted Jan. 16, 2006

Abstract: This work was aimed at gaining understanding of the physical behaviours of the flow and temperature separation process in a vortex tube. To investigate the cold mass fraction's effect on the temperature separation, the numerical calculation was carried out using an algebraic Reynolds stress model (ASM) and the standard k-ε model. The modelling of turbulence of compressible, complex flows used in the simulation is discussed. Emphasis is given to the derivation of the ASM for 2D axisymmetrical flows, particularly to the model constants in the algebraic Reynolds stress equations. The TEFESS code, based on a staggered Finite Volume approach with the standard k-ε model and first-order numerical schemes, was used to carry out all the computations. The predicted results for strongly swirling turbulent compressible flow in a vortex tube suggested that the use of the ASM leads to better agreement between the numerical results and experimental data, while the k-ε model cannot capture the stabilizing effect of the swirl.

Key words: Vortex tube, Cold mass fraction, Swirl flow, Temperature separation, Flow field
doi:10.1631/jzus.2006.A1406 **Document code:** A **CLC number:** TB61$^+$91

INTRODUCTION

Vortex tube is a device for producing hot and cold air when compressed air flows tangentially into the vortex chamber through the inlet nozzles. This causes the vortex and swirl flow movement inside the vortex tube. The air in the middle region of the tube has lower velocity and lower temperature than the inlet air. So the air near the tube wall has higher velocity and higher temperature than the inlet air. The cold air in the core region of the tube flows out through the orifice plate in direction opposite to that of the hot air near the tube wall flowing out through the cone valve as shown in Fig.1a. Generally, the vortex tube can be classified into two types. One is the counter-flow type (often referred to as the standard type) and the other the parallel or uni-flow type, as shown in Figs.1a and 1b, respectively. The vortex tube was first discovered by Ranque (1933; 1934), a metallurgist and physicist who was granted a French patent for the device in 1932, and a United States patent in 1934. Interest in the device was revived by Hilsch, a German engineer, who reported his own comprehensive experimental and theoretical studies aimed at improving the efficiency of the vortex tube (Hilsch, 1947). After that, an experimental study was made by Scheper (1951) who measured the velocity, pressure, and total and static temperature gradients in a Ranque-Hilsch vortex tube, using probes and visualization techniques. Scheper (1951) formulated, following his measurements, a theory based on forced convection heat transfer from the core to the walls in a way similar to a double pipe heat exchanger. A numerical study of a large but short counter-flow vortex tube was conducted by Amitani *et al.*(1983).

‡ Corresponding author

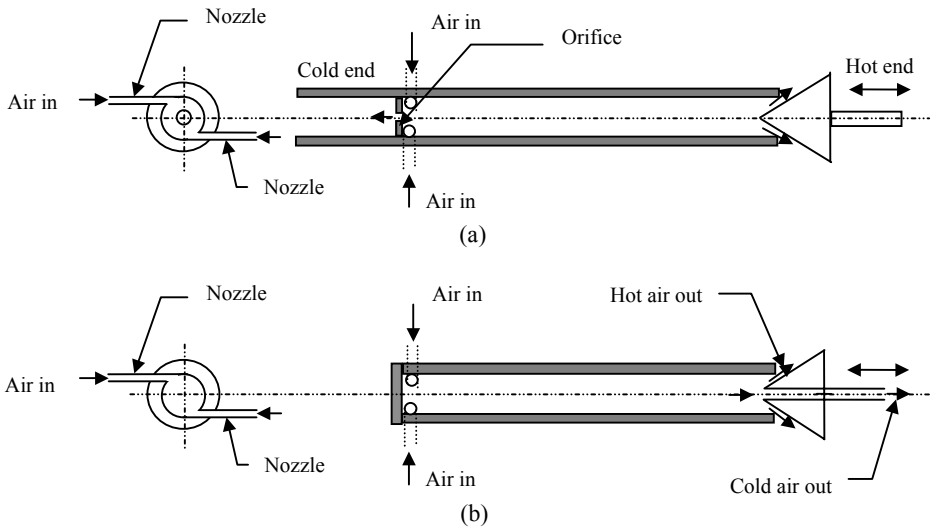

Fig.1 Basic operation of vortex tubes. (a) Ranque-Hilsch standard vortex tube or counter-flow vortex tube; (b) Uni-flow or parallel flow vortex tube

Stephan *et al*.(1984) formulated a general mathematical expression for the energy separation process but this could not be solved because of the complicated system of equations, which led, however, to a similarity relation for the prediction of the cold gas temperature that agreed with the similarity relation obtained by the dimensional analysis (Stephan *et al*., 1983). Nash (1991) analysed the thermodynamics of vortex expansion and evaluated the design limitations of vortex tubes to improve the tube design and carried out experiments with the improved designs, including applications in both high and low temperature cryogenic refrigeration systems.

Ahlborn *et al*.(1994) developed a two-component model to determine the limits of the increase and decrease in temperature within the standard vortex tube. They showed that experimental data with air as working fluid were within the calculated limits and that the flow inside the tube was always subsonic. Frohlingsdorf and Unger (1999) studied the phenomena of velocity and energy separation inside the vortex tube using CFX commercial code with the k-ε model. Promvonge (1999) used a mathematical model for simulating a strongly swirling flow in a uni-flow vortex tube. Promvonge and Eiamsa-ard (2004) experimentally studied the energy separation in a vortex tube with a small entrance. In their experimental results, the use of small entrance could help increase the cold air temperature drop and improve the vortex tube efficiency in comparison with that of original tangential inlet nozzles. Behera *et al*.(2005) investigated the effect of different types of nozzle profiles, and number of nozzles, on temperature separation in the counter-flow vortex tube by computational fluid dynamics and experimental study. Vortex tube numerical modelling was carried out with the code system of Star-CD with "Renormalization Group" (RNG) version of k-ε model. Aljuwayhel *et al*.(2005) reported the energy separation mechanism and flow phenomena within a counter-flow by using the standard k-ε model and the RNG k-ε model. They found that the vortex tube flow field can be divided into three regions: hot flow region (flow that will eventually leave through the hot exit), cold flow region (flow that will eventually leave through the cold exit), and re-circulating region (flow that was entrained within the device).

This research is aimed at numerically studying the flow field and temperature separation in a subsonic vortex tube in order to understand the nature of the Ranque-Hilsch effect by using the algebraic Reynolds stress model (ASM) and the standard k-ε model. The mathematical framework of the present prediction procedure, especially the derivation of Reynolds stresses for compressible flows is introduced. The vortex-tube flow of (Scheper, 1951) is selected in the present study for validation of both the turbulence models.

MATHEMATICAL FORMULATION

Governing equations

For steady compressible flows, the Favre-averaged mean equations of motion, the turbulence kinetic energy (TKE) equation, the energy equation and the equation of state in Cartesian tensor notation can be summarized as:

$$\frac{\partial}{\partial x_i}(\bar{\rho}\tilde{u}_i)=0, \tag{1}$$

$$\frac{\partial(\bar{\rho}\tilde{u}_i\tilde{u}_j)}{\partial x_j}=-\frac{\partial\bar{p}}{\partial x_i}+\frac{\partial}{\partial x_j}(\bar{t}_{ij}+\tau_{ij}), \tag{2}$$

$$\frac{\partial}{\partial x_j}(\bar{\rho}\tilde{u}_j k)=\tau_{ij}\frac{\partial\tilde{u}_i}{\partial x_j}-\bar{\rho}\varepsilon-\overline{u_i''}\frac{\partial\bar{p}}{\partial x_i}+\overline{p'\frac{\partial u_i''}{\partial x_j}}+\frac{\partial}{\partial x_j}\left(\overline{t_{ji}u_i''}-\frac{1}{2}\widetilde{\bar{\rho}u_j''u_i''u_i''}-\overline{p'u_j''}\right), \tag{3}$$

$$\frac{\partial}{\partial x_j}(\bar{\rho}\tilde{u}_j\tilde{E})=\frac{\partial}{\partial x_j}\left(\overline{t_{ji}u_i''}-\overline{p'u_j''}-\frac{1}{2}\widetilde{\bar{\rho}u_j''u_i''u_i''}\right)-\frac{\partial}{\partial x_j}(\bar{q}_{L_j}+\widetilde{\bar{\rho}u_j''h''})+\frac{\partial}{\partial x_j}[\tilde{u}_i(\bar{t}_{ij}+\tau_{ij})]-\frac{\partial}{\partial x_j}(\tilde{u}_j\bar{p}), \tag{4}$$

$$\bar{p}=\bar{\rho}R\tilde{T}=(\gamma-1)(\bar{\rho}\tilde{E}-\bar{\rho}\tilde{u}_i\tilde{u}_i-\bar{\rho}k), \tag{5}$$

where an overbar indicates the mean relative to Reynolds averaging, with a single prime for fluctuation. A tilde and a double prime are corresponding ones for Favre averaging. Also, x_i are the coordinate directions, and ρ is density. u_i are the velocities in the three coordinates directions, k defined by $\bar{\rho}k=\overline{\rho u_i''u_i''}/2=\widetilde{\bar{\rho}u_i''u_i''}/2$ is the turbulence kinetic energy, $\bar{p}$ is the mean pressure, $\tilde{E}\equiv C_v\tilde{T}+\tilde{u}_i\tilde{u}_i/2+\widetilde{u_i''u_i''}/2$ is the mean total energy, and γ is the ratio of specific heats (C_p/C_v). $\bar{q}_L$ is the mean heat flux and the mean viscous stress tensor is approximated as:

$$\bar{t}_{ij}=\bar{\mu}\left(\frac{\partial u_i}{\partial x_j}+\frac{\partial u_j}{\partial x_i}\right)-\frac{2}{3}\bar{\mu}\frac{\partial u_k}{\partial x_k}\delta_{ij}. \tag{6}$$

Finally, $\tau_{ij}=-\overline{\rho u_i''u_j''}=-\widetilde{\bar{\rho}u_i''u_j''}$ is the Favre-averaged Reynolds stress tensor.

The mean conservation equations have resulted in additional terms: τ_{ij}, $\overline{t_{ij}u_j''}$, $\overline{p'u_i''}$, $\widetilde{\bar{\rho}u_i''h''}$ and $\widetilde{\bar{\rho}u_j''u_i''u_i''}/2$ that require modelling. The modelling of some of the unclosed terms in these equations is based on their incompressible models whereas explicit compressible models are required for others. In the present study, two turbulence closure models are used, namely the standard k-ε model and an algebraic stress model (ASM). The k-ε model has already been reviewed in many references such as (Gatski, 1996; Sloan *et al*., 1986; Wilcox, 1993), and it will not be repeated here.

Algebraic Reynolds stress model (ASM)

For simplicity in solving the six Reynolds stresses, Rodi's approximation (Rodi, 1976) is used in this study and the Reynolds stress transport can be expressed in algebraic form as follows:

$$\frac{D\tau_{ij}}{Dt}-T_{ijk,k}=\frac{\tau_{ij}}{\rho k}\left(\frac{Dk}{Dt}-T_{kk,k}\right). \tag{7}$$

Substitution of Reynolds and Favre-averaged transport and the TKE equations into Eq.(7) gives the desired algebraic expression for τ_{ij}:

$$\frac{\tau_{ij}}{\bar{\rho}k}\left(G-\bar{\rho}\varepsilon-\overline{u_i''}\frac{\partial\bar{p}}{\partial x_i}+\overline{p'\frac{\partial u_i''}{\partial x_k}}\right)=G_{ij}+\Phi_{ij}-\frac{2}{3}\delta_{ij}\bar{\rho}\varepsilon+\frac{2}{3}\overline{p'\frac{\partial u_k''}{\partial x_k}}-\overline{u_i''}\frac{\partial\bar{p}}{\partial x_j}-\overline{u_j''}\frac{\partial\bar{p}}{\partial x_i}+\overline{u_i''}\frac{\partial\bar{t}_{jk}}{\partial x_k}+\overline{u_j''}\frac{\partial\bar{t}_{ik}}{\partial x_k}, \tag{8}$$

in which G_{ij} is local production of Reynolds stress, Φ_{ij} is local pressure strain and ε is the TKE dissipation rate. The ASM expressions, after modelling of the unclosed terms, with the pressure dilatation $(\overline{p'\partial u_k''/\partial x_k})$ and the average fluctuating velocity $(\overline{u_i''})$ terms neglected can thus be written as:

$$-\tau_{ij}=\overline{\rho u_i''u_j''}=\frac{2}{3}\delta_{ij}\bar{\rho}k+\frac{\lambda k}{\varepsilon}\left(G_{ij}-\frac{2}{3}\delta_{ij}G-\beta A_{ij}\right), \tag{9}$$

where the empirical constants λ and β, introduced to represent the effect of fluid swirling on gas turbulence, were found to be 0.135 and between 0.0 and 2.2, respectively. The above implicit ASM expressions

can be simplified to obtain an explicit set for easy solution as proposed by Zhang *et al*.(1992) and Nieh and Zhang (1992) for application to a strongly swirling flow. The original algebraic equations of Eq.(9) can therefore be simplified in an explicit form as follows:

$$\left.\begin{aligned}
&\overline{\rho u''v''}=-\mu_{t,xr}\frac{\partial\tilde{u}}{\partial r},\\
&\overline{\rho v''w''}=-\mu_{t,r\theta}r\frac{\partial}{\partial r}\left(\frac{\tilde{w}}{r}\right),\\
&\overline{\rho u''w''}=-\lambda\frac{k}{\varepsilon}\left[\left(\frac{\partial\tilde{w}}{\partial r}+\beta\frac{\tilde{w}}{r}\right)\overline{\rho u''v''}+\frac{\partial\tilde{u}}{\partial r}\overline{\rho v''w''}\right]\\
&\qquad-\lambda\frac{k}{\varepsilon}\overline{\rho u''u''}\frac{\partial\tilde{w}}{\partial x},\\
&\overline{\rho u''u''}=\frac{2}{3}\bar{\rho}k+\frac{2}{3}\lambda\frac{k}{\varepsilon}\left[-2\frac{\partial\tilde{u}}{\partial r}\overline{\rho u''v''}+r\frac{\partial}{\partial r}\left(\frac{\tilde{w}}{r}\right)\overline{\rho v''w''}\right],\\
&\overline{\rho v''v''}=\frac{2}{3}\bar{\rho}k+\frac{2}{3}\lambda\frac{k}{\varepsilon}\left\{\frac{\partial\tilde{u}}{\partial r}\overline{\rho u''v''}+\left[\frac{\partial\tilde{w}}{\partial r}+(2+3\beta)\frac{\tilde{w}}{r}\right]\right.\\
&\qquad\left.\cdot\overline{\rho v''w''}\right\},\\
&\overline{\rho w''w''}=\frac{2}{3}\bar{\rho}k+\frac{2}{3}\lambda\frac{k}{\varepsilon}\left\{\frac{\partial\tilde{u}}{\partial r}\overline{\rho u''v''}-\left[2\frac{\partial\tilde{w}}{\partial r}+(1+3\beta)\frac{\tilde{w}}{r}\right]\right.\\
&\qquad\left.\cdot\overline{\rho v''w''}\right\},
\end{aligned}\right\}\tag{10}$$

in which

$$\mu_{t,xr}=\frac{b_1-a_1b_2r\dfrac{\partial}{\partial r}\left(\dfrac{\tilde{w}}{r}\right)}{1-a_1a_2\dfrac{\partial\tilde{u}}{\partial r}r\dfrac{\partial}{\partial r}\left(\dfrac{\tilde{w}}{r}\right)},\tag{11}$$

$$\mu_{t,r\theta}=\frac{b_2-a_2b_1\dfrac{\partial\tilde{u}}{\partial r}}{1-a_1a_2\dfrac{\partial\tilde{u}}{\partial r}r\dfrac{\partial}{\partial r}\left(\dfrac{\tilde{w}}{r}\right)},\tag{12}$$

where

$$a_1=\frac{\left(\lambda\dfrac{k}{\varepsilon}\right)^2\left[\left(\dfrac{7}{3}+3\beta\right)\dfrac{\tilde{w}}{r}+\dfrac{2}{3}\dfrac{\partial\tilde{w}}{\partial r}\right]}{1+\left(\lambda\dfrac{k}{\varepsilon}\right)^2\left[\dfrac{2}{3}\left(\dfrac{\partial\tilde{u}}{\partial r}\right)^2+(1+\beta)\dfrac{\tilde{w}}{r}\dfrac{\partial\tilde{w}}{\partial r}+A\left(\dfrac{\tilde{w}}{r}\right)^2\right]},$$

$$a_2=\frac{\dfrac{2}{3}\left(\lambda\dfrac{k}{\varepsilon}\right)^2\dfrac{\partial\tilde{u}}{\partial r}}{1+\dfrac{2}{3}\left(\lambda\dfrac{k}{\varepsilon}\right)^2\left[\left(\dfrac{\partial\tilde{w}}{\partial r}\right)^2+(4+6\beta)\dfrac{\tilde{w}}{r}\dfrac{\partial\tilde{w}}{\partial r}+B\left(\dfrac{\tilde{w}}{r}\right)^2\right]},$$

$$b_1=\frac{\dfrac{2}{3}\left(\lambda\bar{\rho}\dfrac{k^2}{\varepsilon}\right)}{1+\left(\lambda\dfrac{k}{\varepsilon}\right)^2\left[\dfrac{2}{3}\left(\dfrac{\partial\tilde{u}}{\partial r}\right)^2+(1+\beta)\dfrac{\tilde{w}}{r}\dfrac{\partial\tilde{w}}{\partial r}+A\left(\dfrac{\tilde{w}}{r}\right)^2\right]},$$

$$b_2=\frac{\dfrac{2}{3}\left(\lambda\bar{\rho}\dfrac{k^2}{\varepsilon}\right)}{1+\dfrac{2}{3}\left(\lambda\dfrac{k}{\varepsilon}\right)^2\left[\left(\dfrac{\partial\tilde{w}}{\partial r}\right)^2+(4+6\beta)\dfrac{\tilde{w}}{r}\dfrac{\partial\tilde{w}}{\partial r}+B\left(\dfrac{\tilde{w}}{r}\right)^2\right]},$$

where

$$A=(1+\beta)\beta,\ B=(1+6\beta+6\beta^2).$$

The above ASM for 2D steady compressible flows were formulated and incorporated in an existing TEFESS code developed by Pun (1992).

Common form for the equations

All the governing partial differential equations can be re-organised and expressed in a standard form that includes the convection, diffusion, and source terms for 2D axisymmetric flows as follows:

$$\begin{aligned}
&\frac{\partial}{\partial x}\left(\bar{\rho}\tilde{u}\phi\right)+\frac{1}{r}\frac{\partial}{\partial r}\left(r\bar{\rho}\tilde{v}\phi\right)-\frac{\partial}{\partial x}\left(\Gamma_{\phi x}\frac{\partial\phi}{\partial x}\right)\\
&\qquad-\frac{1}{r}\frac{\partial}{\partial r}\left(r\Gamma_{\phi r}\frac{\partial\phi}{\partial r}\right)=S_\phi,
\end{aligned}\tag{13}$$

where ϕ, $\Gamma_{\phi x}$, $\Gamma_{\phi r}$ and S_ϕ represent the generalised variables, the exchange coefficients in x and r directions and the source terms, respectively.

Solution procedure

In the present computation the Favre-averaged Navier-Stokes equations, Eqs.(1) and (2); the TKE equation, Eq.(3); the energy equation, Eq.(4); the equation of state, Eq.(5); the TKE dissipation rate equation, are solved numerically by a control-volume finite-difference method (Patankar, 1980) together with the turbulence model equations, Eq.(10) for the ASM. The SIMPLE algorithm is utilised for pressure-velocity de-coupling and iteration. The discretization of the governing equations is accomplished by means of the upwind scheme and the source term linearisation is accomplished on a staggered grid cell. The underrelaxation iterative TDMA line-by-line sweeping technique is used for solving the resultant finite-difference equations. Due to the highly non-

linear and coupling features of the governing equations for swirling flows, lower underrelaxation factors ranging from 0.001 to 0.2 were chosen for the three velocity components to ensure the stability and convergence of the iterative calculation. The wall function is used at the grid nodes along the walls.

VORTEX TUBE OF (SCHEPER, 1951)

This case was designed to examine the flow characteristics and energy separation effect in a vortex tube for three values of the cold mass flow ratio ($\dot{m}_c/\dot{m}_{in}$), namely, 0.0, 0.26 and 0.78. Scheper (1951)'s measurements were made in a lucite tube with inside diameter of 0.0381 m and length of 0.9144 m. The air entered the tube tangentially through a single 0.00635 m diameter inlet nozzle and left the tube through both a cone-shaped hot valve and a 0.0127 m diameter cold orifice. Experimental profiles of total velocity, static temperature and total temperature were obtained at a single axial station, x/D_o= 2, for cold mass ratios 0.0 and 0.78 and at three axial stations, x/D_o=2.0, 3.6 and 16.93, for cold mass ratio 0.26, with the nozzle supply pressure p_o=2 atm (abs.). Details of the tube geometry and fluid properties for the case are summarised in Table 1. Unfortunately, the mass flow rate and pressure profiles are not available and the single measured profile provided is not sufficient for an extrapolation procedure. Data were assumed for this case. For example, pressure at the discharge valve exit was assumed to be equal to atmospheric pressure and used as a reference pressure for the three cold mass flow ratios shown in Table 2. The mass flow rate was estimated from the relations among the supply pressure (p_o), the nozzle area (A_n) and the mass flow rate ($\dot{m}_{in}$) as suggested by Hilsch (1947).

Table 1 Data on vortex flow measured by Scheper (1951)

Parameter	Value
Tube characteristics (hot tube only)	
Tube length, L (m)	0.9144
Tube diameter, D_o (m)	0.0381
No. of Nozzle	1
Nozzle diameter, d_n (m)	0.00635
Cold orifice diameter, d_c (m)	0.0127
Discharge hole	–
L/D_o ratio	24
Inlet fluid properties	
Fluid	Air
Temperature, T_{in} (K)	290.95
Pressure before nozzle, p_o (Pa)(gage)	1.01×10^5
Flow conditions	
Mass flow rate $\dot{m}_{in}$ (kg/s)	0.04265
Cold mass flow $\dot{m}_c$ (kg/s)	0, 0.01108, 0.03327
Hot mass flow $\dot{m}_h$ (kg/s)	0.04265, 0.03157, 0.00938

Table 2 Input data measured by Scheper (1951)

V_n (m/s)	w_n (m/s)	v_n (m/s)	ρ_n (kg/m^3)	T_n (K)	l_s (m)
230	200	76	1.55	290.95	0.001

Calculations using the inlet assumed data described above with both the standard k-ε model and the ASM were first carried out for the zero cold mass flow rate ratio. A slight adjustment of the assumed inlet velocities and mass flow rate was made in order to make the predicted results conform closer to experimental profiles. The adjusted inlet data of the zero cold mass flow ratio case were then applied to the other cold mass flow rate ratios and presented in Table 1.

BOUNDARY CONDITIONS

The calculated mean quantities were compared with available measurements at selected stations. Basic assumptions for all the computations of the particular vortex-tube flows were made as follows: 2D axisymmetrical, subsonic flow inside the vortex tube, uniform flow properties at the inlet and ideal gas. Since the system is assumed to be an axisymmetric flow, only half of the flow domain needs to be considered throughout and special treatment for the flow at the inlet must be made for the computations. At the inlet, a circumferential slot is assumed instead of the actual inlet nozzle. For simplicity in the present computation the cone-shaped valve used as a discharge valve at the exit is replaced with a block valve. In addition, owing to lack of wall temperature information, the influences of the wall temperature on the predictions were investigated. Because of the complex geometry of the flow, data for boundary conditions should be carefully considered in order to make computations realistic. Details of data for the vortex-tube flows are given below.

Inlet

Properties at the inlet are usually obtained from experimental data, analysis, or estimation. It is very rare that all the boundary conditions required are available from experiment. Quantities of primary importance here are the velocity components normal and tangential to the inlet. In axisymmetric flows, the swirl component must also be known. The counter-flow vortex-tube type generally has an entrance block with an orifice and a control valve. Compressed gas enters the vortex tube tangentially through one or more nozzles. Most experiments provide inlet data such as pressure p_o, temperature T_o and mass flow rate just before the nozzle. Unfortunately, they cannot be used as input data for computations which need the data at the nozzle exit stage. Little is known about the static pressure p_n, temperature T_{in}, and velocity V_n, at the nozzle outlet. Those values may be obtained by extrapolation from their experimental profiles inside the tube to the nozzle exit location. Thus, this practice is adopted for the velocities; the total temperature at the nozzle exit is obtained by assuming an adiabatic nozzle, so that the total energy is conserved throughout the nozzle. Note that the static pressure values inside the flow field are calculated relative to the value at a reference point, for which measurement is available. Density at the inlet is calculated from the continuity equation:

$$\rho_n = \frac{\dot{m}_{in}}{A_n V_n}, \tag{14}$$

where A_n, ρ_n and V_n are the total area, density and average velocity at the nozzle exit respectively and $\dot{m}_{in}$ represents the total air mass flow rate. However, in the case where the total mass flow rate is not available but the static pressure and the static temperature profiles inside the tube are provided, the equation of state is used to estimate the density at the inlet ($\rho_n=p_s/(RT_s)$), the inlet static pressure and temperature used in the equation being obtained by extrapolation from the experimental profiles.

For axisymmetric flow, a circumferentrial slot at the inlet is used instead of the nozzle(s). The equivalent width of the slot, l_s, is calculated from the conservation of mass with the relation below:

$$l_s = \frac{\dot{m}_{in}}{\pi D_o \rho_n v_n}, \tag{15}$$

where l_s, D_o and v_n are the slot width, the vortex-tube diameter and the inlet radial velocity respectively (Fig.2), where

$$v_n = \sqrt{V_n^2 - w_n^2}, \tag{16}$$

in which w_n is the tangential velocity at the inlet. The values of V_n and w_n in the present computations were obtained by extrapolation from experimental measurements. The dynamic viscosity generally is a function of the temperature. However, in the present computations, it is assumed to be uniform throughout (equal to μ at the inlet temperature) because the temperature change in the vortex tube is not large.

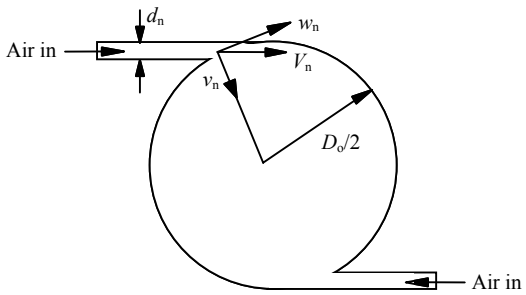

Fig.2 Inlet properties of the vortex tube

Wall

All the measurements selected were given without reference to the environment of the tube and it is believed that invariably the tube was exposed without insulation to the ambient temperature during the experimental investigation. Since the vortex tubes were made of plexiglas or lucite whose properties offered some insulation, the correct wall temperature should lie between the adiabatic wall and constant ambient temperatures. In the present computations, the temperature measured near the wall at all locations differed from the ambient temperature and an adiabatic wall condition was, therefore, applied.

Outlet

As mentioned earlier, the cone-shaped valve used as a discharge control at the exit was replaced with a block valve for counter-flow vortex-tube type. There are two exits involved, one for the cold air was treated with the conventional setting of zero gradient of variables while the other, the discharge valve, with the prescription of flat axial velocity profile at the hot tube

outlet. The prescribed flat axial velocity profile at the hot tube exit was used to control the mass rate of flow through the discharge valve. Therefore, the value of the profile depends on the cold mass flow rate ratio needed. The preliminary test in the present study to investigate the sensitivity of solutions to exit boundary conditions with a block valve and a fully open valve showed that the predictions with both the turbulence models were insensitive to the exit conditions.

RESULTS AND DISCUSSION

Numerical computations were performed on a 60×25 grid for the zero cold mass flow rate ratio and on an 80×25 grid with non-uniform distributions for cold mass flow rate ratios of 0.26 and 0.78. A test was conducted showing that grid-independence solutions were achieved with both the grids. A first-order numerical scheme, the upwind, was used.

Flow field

Figs.3a~3c compare the predicted total velocity profiles using the k-ε model and the ASM with experimental data for the cold mass flow rate ratios of 0.0, 0.26 and 0.78 respectively. It was found that results with the k-ε model show the decay to a solid-body type shape for all the cold mass flow rate ratios, while those of the ASM enable conformity to the measurements quite well. The solutions with both the turbulence models were slightly under-predicted near the tube wall region. In general, the ASM produces solutions better than the k-ε model results.

Temperature field

Zero cold mass flow rate ratio: Figs.4a and 4b show the axial variations of total temperature at locations r/R=0.1667 and 0.8333, respectively, using both the turbulence models for the zero cold mass flow rate ratio. It is seen that, except in the region near the inlet (x/D_o<2), the ASM predictions accord very well with the experimental data while the k-ε model gives under-predicted results. Overall, the ASM predictions yield closer agreement with the data than those with the k-ε model. It is believed that if a 3D flow calculation is used and important data at the inlet are available, the ASM results near the inlet region would improve significantly.

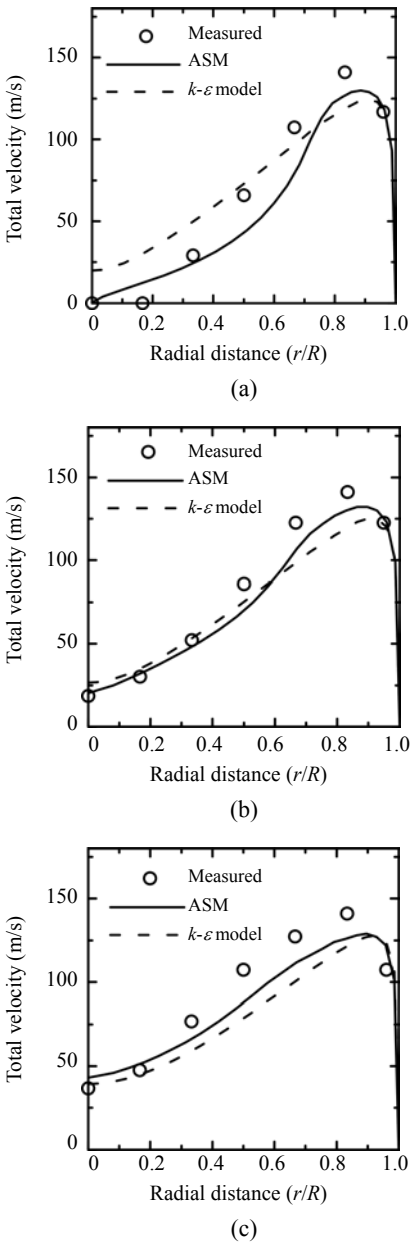

Fig.3 Comparison of predicted velocity profiles at various cold mass ratios with measurements of (Scheper, 1951) (x/D_o=2). (a) m_c/m_{in}=0.0; (b) m_c/m_{in}=0.26; (c) m_c/m_{in}=0.78

It is evident from Fig.5a that predicted radial distributions of static temperature using both the turbulence models are in good agreement with measurements. The ASM results mimic the measured data very well, except for the small region near the wall, while the k-ε model gives slightly under-predicted results. For this case, the measurements showed a trend of gradual increase in static tempera-

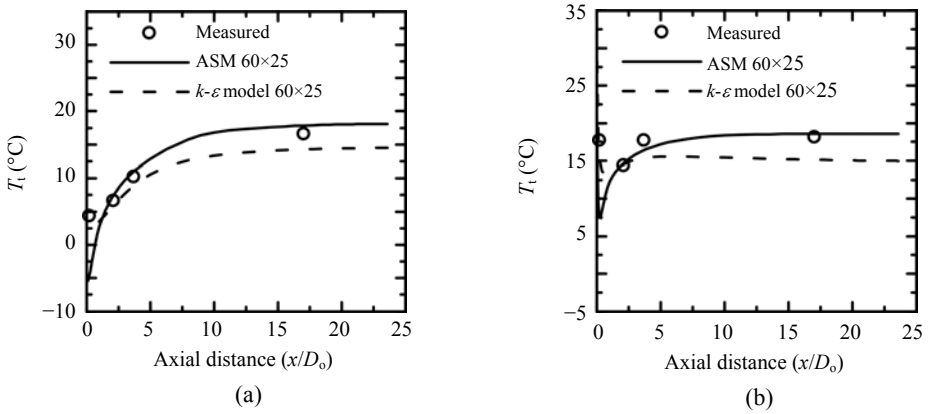

Fig.4 Axial profiles of predicted total temperature with measurements of (Scheper, 1951) for zero cold mass ratio (m_c/m_{in}=0.0, T_{in}=17.8 °C). (a) r/R=0.1667; (b) r/R=0.8333

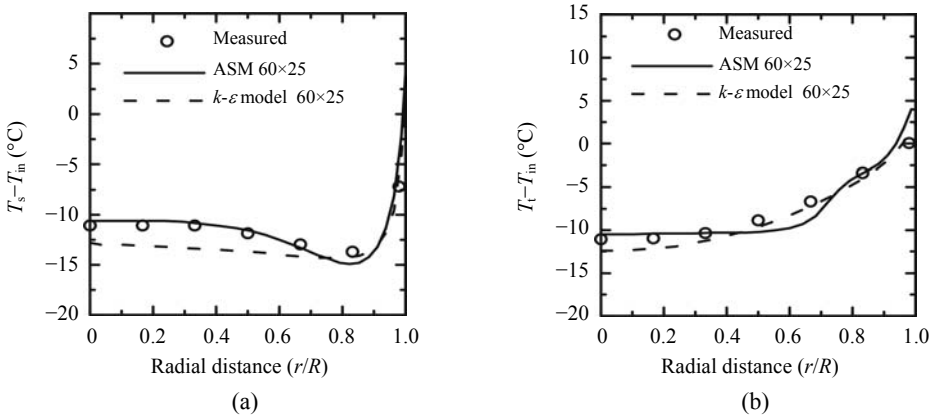

Fig.5 Radial profiles of predicted temperature with measurements of (Scheper, 1951) for zero cold mass ratio (m_c/m_{in}=0.0, T_{in}=17.8 °C, x/D_o=2). (a) Static; (b) Total

ture in the radially inward direction in the core region. The predicted radial profiles of total temperature using the k-ε model and the ASM along with the measurements are given in Fig.5b showing that predictions with both the turbulence models are in good agreement with the experimental data. The lowest temperature in the tube core is well predicted with the ASM but slightly under-predicted with the k-ε model. The peak values near the tube wall are slightly over-predicted with both the turbulence models.

Cold mass flow rate ratio of 0.78: Figs.6a and 6b compare, respectively, the calculated radial profiles of static and total temperatures using the k-ε model and the ASM with the measurements for the cold mass flow rate ratio of 0.78. Comparisons were made only at the station x/D_o=2 where the experimental data are available. Fig.6b suggests that the ASM predictions are in good agreement with the measured data whereas the k-ε model yields under-predicted results. The minimum and peak values of total temperature with the ASM are well predicted. For the static temperature profiles, although results with both the turbulence models are under-predicted, their trends follow the measurements very well. Further consideration revealed that the ASM results, compared to k-ε model results, are in closer agreement with the experimental data.

Cold mass flow rate ratio of 0.26: Figs.7a and 7b compare, respectively, the predicted radial profiles of static and total temperatures using the k-ε model and the ASM with the measurements for the cold mass flow rate ratio of 0.26. For this ratio, the experimental data were available at three stations, x/D_o=2.0, 3.6 and 16.93. It is seen that for the static temperature profiles, the ASM predictions are in close agreement with the measured data whereas the k-ε model under-predicts

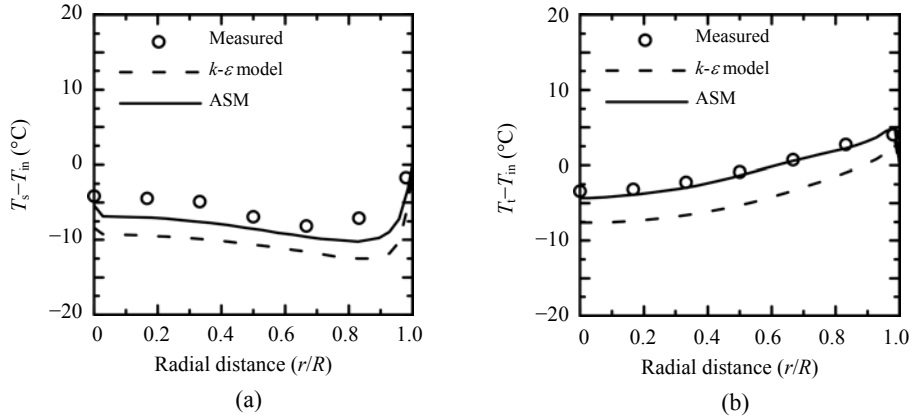

Fig.6 Comparison of predicted temperature profiles with measurements of (Scheper, 1951) for cold mass ratio (m_c/m_{in}=0.78, x/D_0=2, T_{in}=17.8 °C). (a) Static; (b) Total

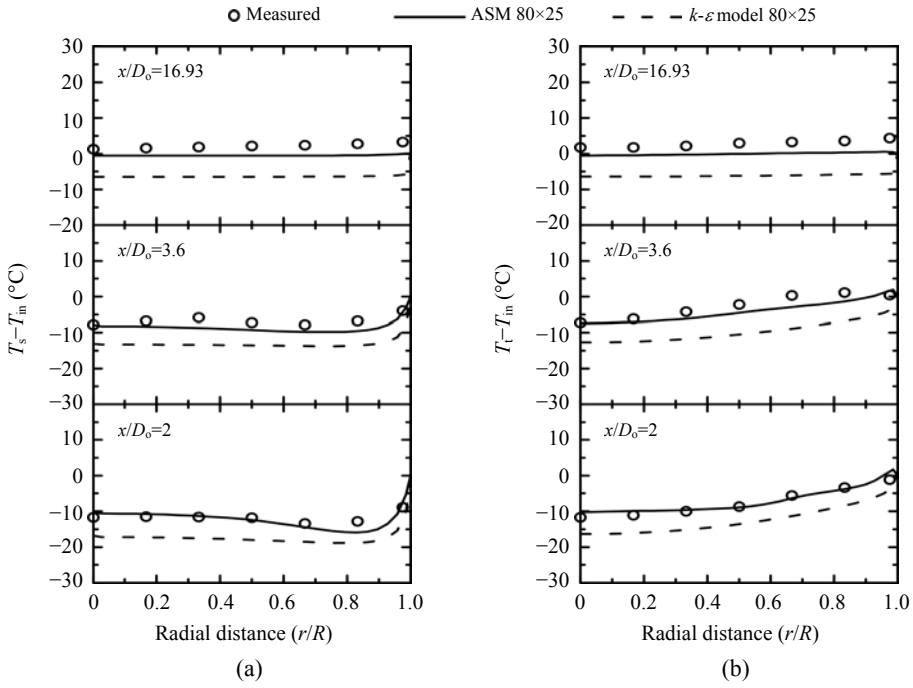

Fig.7 Comparison of predicted temperature profiles with measurements of (Scheper, 1951) for cold mass ratio (m_c/m_{in}=0.26, T_{in}=17.8 °C). (a) Static; (b) Total

the results at all the stations. The minimum and peak values of static temperature with the ASM are fairly well-predicted. Again, the trend of the predicted results with both the turbulence models mimics the experimental profiles very well. For the total temperature profiles, it was also found that the ASM results, compared to k-ε model results, displayed closer agreement with the experimental data at all the stations. The lowest and highest temperatures were well predicted with the ASM but under-predicted with the k-ε model for all three stations.

For this calculated results, it is worth noting that the validations for the three cold mass flow ratios are not expected to yield good agreement with measurements because of the lack of important measured data for the inlet boundary condition. The same assumed inlet data set as used in the present computations may be unsuitable for all the cold mass flow ratios. This was, for instance, confirmed by Negm *et al.*(1988) who reported that the mass flow rate in a

vortex tube varied slightly with cold mass flow rate ratios for the same inlet supply pressure and a maximum mass flow rate was found for the zero cold mass flow rate ratio. However, the motivation for this test case was mainly to show that reliable qualitative trends can be obtained between predictions and experimental static temperature profiles which were measured directly, adding confidence in the models used.

CONCLUSION

Numerical simulations with both the standard k-ε model and the ASM were conducted to predict compressible vortex-tube flows. Major findings can be summarised as follows:

The computations showed that temperature separation inside a vortex tube exists. Predictions with the ASM are in closer agreement with measurements than those with the k-ε model for the quantities compared. In terms of overall local flow properties and temperature, the ASM has better conformity to the experimental data due to its ability to introduce non-isotropic turbulence effects.

References

Ahlborn, B., Keller, J.U., Staudt, R., Treitz, G., Rebhan, E., 1994. Limits of temperature separation in a vortex tube. *J. Physics D: Applied Physics*, **27**(3):480-488. [doi:10.1088/0022-3727/27/3/009]

Aljuwayhel, N.F., Nellis, G.F., Klein, S.A., 2005. Parametric and internal study of the vortex tube using a CFD model. *International Journal of Refrigeration*, **28**(3):442-450. [doi:10.1016/j.ijrefrig.2004.04.004]

Amitani, T., Adachi, T., Kato, T., 1983. A study on temperature separation in a large vortex tube. *Trans. JSME*, **49**:877-884.

Behera, U., Paul, P.J., Kasthurirengan, S., Karunanithi, R., Ram, S.N., Dinesh, K., Jacob, S., 2005. CFD analysis and experimental investigations towards optimizing the parameters of Ranque-Hilsch vortex tube. *Int. J. Heat and Mass Transfer*, **48**(10):1961-1973. [doi:10.1016/j.ijheatmasstransfer.2004.12.046]

Frohlingsdorf, W., Unger, H., 1999. Numerical investigations of the compressible flow and the energy separation in the Ranque-Hilsch vortex tube. *Int. J. Heat and Mass Transfer*, **42**(3):415-422. [doi:10.1016/S0017-9310(98)00191-4]

Gatski, T.B., 1996. Turbulent Flows: Model Equations and Solution Methodology. *In*: Peyret, R. (Ed.), Handbook of Computational Fluid Mechanics. Academic Press Ltd., London.

Hilsch, R., 1947. The use of expansion of gases in a centrifugal field as a cooling process. *Review of Scientific Instruments*, **18**(2):108-113. [doi:10.1063/1.1740893]

Nash, J.M., 1991. Vortex Expansion Devices for High Temperature Cryogenics. Proceedings of the Intersociety Energy Conversion Engineering Conference, **4**:521-525.

Negm, M.I.M., Serag, A.Z., Abdel Ghany, S.M., 1988. Performance characteristics of energy separation in double stage vortex tubes. *Modelling, Simulation & Control B: Mechanical & Thermal Engineering, Materials & Resources, Chemistry*, **14**:21-32.

Patankar, S.V., 1980. Numerical Heat Transfer and Fluid Flow. Hemisphere Publishing Incorp., Washington DC.

Promvonge, P., 1999. Numerical Simulation of Turbulent Compressible Vortex-Tubes Flow. Proceedings of the 3rd ASME/JSME Joint Fluids Engineering Conference. San Francisco, California.

Promvonge, P., Eiamsa-ard, S., 2004. Experimental investigation of temperature separation in a vortex tube refrigerator with snail entrance. *ASEAN Journal on Science & Technology for Development*, **21**:297-308.

Pun, W.M., 1992. An Introduction to the TEFESS Code. Internal Report, Mechanical Engineering Department, Imperial College of Science, Technology & Medicine.

Ranque, G.J., 1933. Experiments on expansion in a vortex with simultaneous exhaust of hot air and cold air. *Le Journal de Physique et le Radium (Paris)*, **4**:112-114, S-115. Also translated as General Electric Co., Schenectady Works Library, T.F. 3294 (1947).

Ranque, G.J., 1934. Method and Apparatus for Obtaining from a Fluid under Pressure Two Outputs of Fluid at Different Temperatures. US Patent No. 1,952,281.

Rodi, W.A., 1976. New algebraic relations for calculating the Reynolds stresses. *Z. Angew. Math. Mech.*, **56**:T219-T221.

Scheper, G.W., 1951. The vortex tube; internal flow data and a heat transfer theory. *J. ASRE, Refrigerating Engineering*, **59**:985-989.

Sloan, D.G., Smith, P.J., Smoot, L.D., 1986. Modeling of swirl in turbulent flow system. *Progr. Energy Combust. Sci.*, **12**(3):163-250. [doi:10.1016/0360-1285(86)90016-X]

Stephan, K., Lin, S., Durst, M., Huang, F., Seher, D., 1983. An investigation of energy separation in a vortex tube. *Int. J. Heat Mass Transfer*, **26**(3):341-348. [doi:10.1016/0017-9310(83)90038-8]

Stephan, K., Lin, S., Durst, M., Huang, F., Seher, D., 1984. A similarity relation for energy separation in a vortex tube. *Int. J. Heat Mass Transfer*, **27**(6):911-920. [doi:10.1016/0017-9310(84)90012-7]

Wilcox, C.D., 1993. Turbulent Modelling for CFD. DCW Industries Inc., California.

Zhang, J., Nieh, S., Zhou, L., 1992. A new version of algebraic stress model for simulating strongly swirling turbulent flows. *J. Numerical Heat Transfer*, **22**:49-62.